NASA Technical Memorandum 102130

Subtle Porosity Variation in the $YBa_2Cu_3O_{7-x}$ High-Temperature Superconductor Revealed by Ultrasonic Imaging

D.J. Roth and E.R. Generazio
National Aeronautics and Space Administration
Lewis Research Center
Cleveland, Ohio

D.B. Stang
Sverdrup Technology, Inc.
NASA Lewis Research Center Group
Cleveland, Ohio

and

A.F. Hepp
National Aeronautics and Space Administration
Lewis Research Center
Cleveland, Ohio

January 1990

Trade names or manufacturers' names are used in this report for identification only. This usage does not constitute an official endorsement, either expressed or implied, by the National Aeronautics and Space Administration.

SUBTLE POROSITY VARIATION IN THE $YBa_2Cu_3O_{7-x}$ HIGH-TEMPERATURE SUPERCONDUCTOR REVEALED BY ULTRASONIC IMAGING

D.J. Roth and E.R. Generazio
National Aeronautics and Space Administration
Lewis Research Center
Cleveland, Ohio 44135

D.B. Stang
Sverdrup Technology, Inc.
NASA Lewis Research Center Group
Cleveland, Ohio 44135

and

A.F. Hepp
National Aeronautics and Space Administration
Lewis Research Center
Cleveland, Ohio 44135

Summary

This study reports on characterization of global porosity variation within a nominally 93-percent-dense specimen of $YBa_2Cu_3O_{7-x}$ high-temperature superconductor. With a computer-controlled scanning system, precision ultrasonic velocity measurements were obtained at 100-μm increments over an 8- by 8-mm area of the $YBa_2Cu_3O_{7-x}$ specimen. The measurements were used to form a color map of velocity variation across the scanned region of the specimen. Subtle velocity variation on the order of 1 percent was observed. The specimen was shown by experimental methods to be single-phase, untextured, and free of nonuniform residual microstresses. From this knowledge and an established velocity-density relationship, a likely conclusion is that the observed velocity variations are solely due to porosity variations of similar magnitude. Locating these subtle porosity variations is critical since they can result in an order of magnitude variation in critical current density J_c for dense YBCO specimens. Thus, mapping the global porosity distribution within $YBa_2Cu_3O_{7-x}$ may reveal regions that have poorer superconducting properties. In this study ultrasonic velocity results are translated into useful microstructural information for the material scientist.

Introduction

The last several years have seen the remarkable development of a new class of ceramics that exhibit superconductivity to unprecedentedly high temperatures (refs. 1 to 3). As is the case for most materials, the microstructure has a significant effect on the physical properties exhibited by the high-T_c ceramics. Microstructure-property relationships for these materials are currently being investigated (refs. 4 to 11). These relationships need to be carefully defined in order to improve or at least control the electrical, magnetic, and mechanical properties of the high-T_c ceramics.

The microstructure-property relationships for the high-T_c materials that have been investigated to date are based on global sample-to-sample variation (for example, the properties of a large-grained, low-density sample versus those for a fine-grained, high-density sample). It is known that microstructural homogeneity within a (ceramic, metal, or polymer) material sample is generally necessary for the sample to exhibit uniform, consistent, and predictable physical behavior (refs. 12 to 14). In structural ceramics such as SiC, even small variations in porosity fraction, phase composition, preferred granular orientation (texture), and residual stress across a specimen can significantly affect mechanical performance. The

effects of similar within-sample inhomogeneity on the electrical, magnetic, and mechanical behavior of the high-T_c ceramics need to be determined. An important step in this determination is accurate and precise structural characterization on both a local (grain size) and global (sample size) scale to quantify the level of inhomogeneity. Previous studies have investigated compositional variability over local (100- by 100-μm) regions of $YBa_2Cu_3O_{7-x}$ (YBCO) superconductor specimens (refs. 6 and 15).

This report describes the characterization of global porosity variation within a nominally 93-percent-dense specimen of YBCO that was shown experimentally to be single-phase, untextured, and free of nonuniform residual microstress. High-frequency ultrasound was used to probe the YBCO microstructure. With a computer-controlled precision acoustic scanning system (PASS) (refs. 16 to 18), ultrasonic velocity was measured at 100-μm increments over an 8- by 8-mm area of the YBCO specimen. The measurements were used to construct a detailed color map of porosity variation across the scanned region of the specimen. Conventional x-ray radiography was also used to examine the sample for porosity variations.

Background

Porosity Effects For YBCO

Porosity, phase purity, and texture are microstructural features that critically affect the electrical properties of the high-T_c materials. Previous studies have shown that an increased presence of voids and second phases in polycrystalline samples of YBCO generally limits critical current densities J_c (refs. 4, 5, 8, and 10) and diamagnetic susceptibilities (ref. 11), and increases (worsens) the transition width ΔT_c (refs. 7 and 19). The existence of pores and/or second-phase particles at grain boundaries is thought to cause weak coupling between high-J_c grains, thus limiting the bulk transport J_c (refs. 8, 20, and 21).

Even slight variations in porosity may have a significant effect on electrical and magnetic performance. Alford (refs. 4 and 5) has shown that porosity variations on the order of 1 percent in polycrystalline YBCO samples can result in an order of magnitude variation in J_c. This effect is thought, on the basis of present processing methods, to result from the existence of an optimum density near 92 percent of theoretical for YBCO to exhibit maximum J_c. As YBCO density increases from approximately 70 to 92 percent, an increasing trend in J_c occurs due to increased grain connectivity. At densities above 92 percent, pore closure forces oxygen transport to occur by relatively slow bulk diffusion, and a much greater annealing time is required to achieve the necessary oxygenation. An insufficient annealing period may result in oxygen-deficient regions in the final YBCO product, thereby leading to dramatically decreased J_c and diamagnetic response.

The presence of porosity and its local distribution in YBCO materials may also be important for flux pinning (ref. 22), since recent results point to a conventional model of type II superconductivity for YBCO (refs. 23 to 25). Pores within grains of YBCO act as effective pinning centers (refs. 26 and 27), and increased flux pinning leads to increased J_c (ref. 28).

The mechanical properties of the high-T_c materials and the associated microstructural effects must also be taken into account. Superconductors within high-field magnets can be subjected to large mechanical loads due to thermal expansion mismatch between different materials in the magnet structure and generated Lorentz forces (ref. 29). The same microstructural features of porosity, second phases, and texture that affect electrical performance also have a significant effect on mechanical properties such as stiffness, strength, and toughness of YBCO (refs. 5, 6, and 9). Alford (ref. 5) and Blendell (ref. 6) show that an optimum density also may exist for polycrystalline YBCO to achieve maximum strength and stiffness.

Since small variations in density (porosity fraction) can have such a crucial effect on the properties of YBCO, knowledge and control of the global porosity distribution within YBCO specimens is extremely important.

Ultrasound as a Microstructural Probe

Ultrasound is a sensitive probe of microstructure since it interacts (via absorption and scattering) with grains, pores, and inclusions in polycrystalline materials. Furthermore, ultrasonic techniques offer nonintrusive means for examining microstructures. Ultrasonic velocity and attenuation measurements have been used previously to examine and image microstructural features such as grain and porosity distributions in metals and ceramics (refs. 16, 17, and 30 to 38). At least 120 studies have been reported in the last 3 yr concerning ultrasonic analysis of the high-T_c superconductors (ref. 39).

In polycrystalline ceramics, ultrasonic velocity is strongly dependent on texture, phase concentration, and pore concentration; but it is weakly or not at all dependent on grain size, pore size, and pore orientation (refs 30, 35, and 40). Velocity has also been shown to be sensitive to residual stress states in polycrystalline metals (refs. 41 to 43). In addition, velocity may be affected by the presence of twin bands. Variations in the microstructural condition can be inferred by measuring ultrasonic velocity at regular intervals across a specimen and then constructing a map (image) of the measurements. Variations in pore concentration can be imaged if the specimen is single-phase and randomly textured (and thus randomly twinned) and residual stresses are either negligible or uniformly distributed.

Ultrasonic Velocity of YBCO

In figure 1 previously measured longitudinal-wave ultrasonic velocities for polycrystalline YBCO samples at room temperature are plotted as a function of percent porosity (refs.

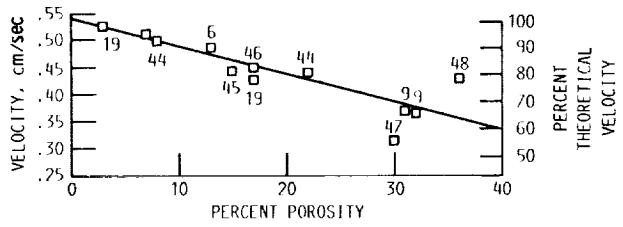

Figure 1.—Ultrasonic velocity as a function of percent porosity for YBCO. Number indicates reference; unnumbered data point is that of the authors.

6, 9, 19, and 44 to 48). The line drawn in the figure is a least-squares fit of the data points. Figure 1 indicates that ultrasonic velocity decreases with increasing percent porosity for YBCO. This result is in agreement with that previously obtained for SiC polycrystalline ceramics (refs. 30 and 35). If

$$\text{percent theoretical velocity} = (V_p / V_0) \times 100 \qquad (1)$$

where V_p is the velocity corresponding to some percent porosity along the least-squares-fit line, and V_0 is the velocity at zero-percent porosity determined from the least-squares-fit line, or 0.54 cm/μsec, a 1-percent change in ultrasonic velocity can be seen to correspond approximately to a 1-percent change in porosity (and density) for YBCO.

Investigation

Specimen

A YBCO disk 24.2 mm in diameter and 4 mm thick was obtained from W.R. Grace & Co. (Columbia, MD 21044). Table I summarizes the preliminary sample characterization. The density, measured from sample dimensions and weight, was 93 percent (5.94 g/cm^3) of theoretical. With the four-contact method, the YBCO specimen achieved zero resistance at a temperature of 87 K. In addition, a small permanent magnet became suspended over the disk at 77 K (i.e., the Meissner effect (refs. 49 and 50) was observed) in the as-received state and on completion of the experiment. The disk was ground to a thickness of 2.800 ± 0.001 mm and was polished (on one side) with 3- and 0.5-μm diamond paste to a final thickness of 2.788 ± 0.002 mm in preparation for ultrasonic scanning.

On completion of the ultrasonic scanning, the disk was sectioned parallel to and perpendicular to the top surface at several locations within the ultrasonically scanned region. The disk was prepared for photomicrographs by 40-, 20-, 6- and 3-μm rough polishings followed by 3-, 1- and 0.5-μm final polishings. A nonaqueous lubricant was used during all finishing steps so as to preserve the superconducting properties of the disk (refs. 51 and 52). Some microcracking was apparent on and very near the disk surface both in the as-received condition and after finishing. No significant microcracking of the bulk was noted.

Grain and porosity distribution photomicrographs were obtained at near-surface and bulk locations within the ultrasonically scanned area. Representative photomicrographs of the grain and porosity distributions of the YBCO sample appear with table I. Porosity was of the isolated, noninterconnecting type that is characteristic of such dense specimens of YBCO. Pores ranged in size from approximately 1 to 20 μm.

A total of about 1100 grains (approximately 360 grains in each of three directions 45° apart) were sampled by using the Heyn intercept method (ASTM E112–85) to obtain average size and to determine if preferred grain orientation was present in any plane in the sample. Twin bands were evident within the grains of the YBCO specimen. Nonequiaxed grains ranging from approximately 2 to 150 μm were apparent. The mean grain size obtained for the YBCO specimen was 5.99 ± 0.76 μm (one standard deviation). The mean grain sizes in each of three directions 45° apart were 5.69 ± 0.65 μm, 5.98 ± 0.82 μm, and 6.25 ± 0.96 μm. When taking into account the measurement uncertainty and the calculated standard deviations, the mean grain sizes were approximately equal for the three directions, thus indicating a randomly textured (and thus randomly twinned) material.

X-ray diffraction at surface and bulk locations of the YBCO disk determined the phases and stress state present (refs. 53 and 54). Data were collected with a computer-controlled diffractometer using $CuK(\alpha)_1$ radiation. Approximately 1 mm^2 of the material was sampled by the x-ray beam. Garlick (NASA Lewis Research Center, Cleveland, OH, personal communication) estimated that this experimental configuration can reveal phases in quantities as low as 0.5 to 1 percent by volume. X-ray diffraction results revealed that only the YBCO superconducting (orthorhombic) phase was present, with the unit cell parameters $a_o = 3.83 \pm 0.01$ Å, $b_o = 3.89 \pm 0.01$ Å, and $c_o = 11.68 \pm 0.03$ Å (ref. 55). Optical ellipsometry measurements confirmed that surface areas of the YBCO disk contained oxygen stoichiometry characteristic of the orthorhombic phase (ref. 56).

Machining and grinding operations are believed to result in nonuniform residual microstresses at the surface of ceramics (ref. 57). The microstrains resulting from nonuniform residual microstresses cause a broadening that is over and above the instrumental breadth of the x-ray diffraction line. This characteristic line broadening was not evident in the x-ray diffraction patterns for the YBCO specimen, thus indicating a negligible state of nonuniform residual microstress at surface and bulk locations.

From preliminary characterization, the YBCO disk appears to be single-phase (orthorhombic YBCO), randomly textured, and free of nonuniform residual microstress. A reasonable conclusion, based on these considerations, is that porosity fraction is indeed the microstructural feature being examined in the YBCO disk with radiographic attenuation and ultrasonic velocity measurements.

I-a. POROSITY DISTRIBUTION

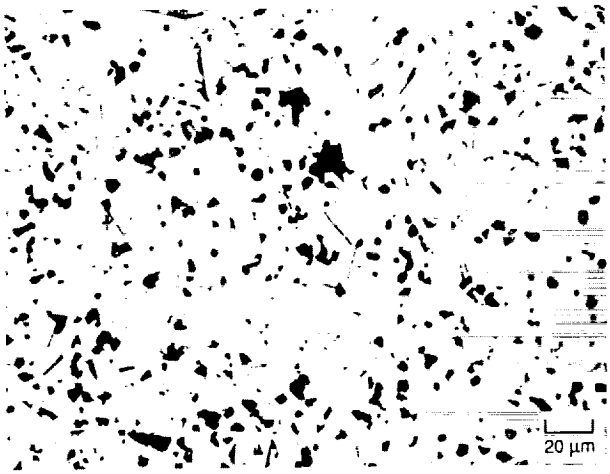

ORIGINAL PAGE
COLOR PHOTOGRAPH

I-b. GRAIN DISTRIBUTION

TABLE I.—PRELIMINARY CHARACTERIZATION OF $YBaCu_3O_{7-x}$ SPECIMEN

Disk dimensions, mm	
Diameter	24.2
Thickness	2.788 ± 0.002
Density, g/cm^3	5.94
Percent theoretical	93
Porosity distribution [a] (See I-a)	
Type	isolated
Size, μm	1 to 20
Grain distribution [b] (See I-b)	
Texture	random
Size, μm	2 to 150
Mean, μm	5.99 ± 0.76
Phase purity	
Oxygen content, atoms [c] (See I-c)	≥ 6.9
Unit cell dimension, Å [d] (See I-d)	
a_o	3.89 ± 0.01
b_o	3.83 ± 0.01
c_o	11.68 ± 0.03
Crystal structure	orthorhombic
Nonuniform residual stress [d] (See I-d)	none
Superconducting transition temperature [e], K (See I-e)	87

[a] Determined from optical micrograph of metallographically polished section (black spots indicate porosity).
[b] Determined from optical micrograph of metallographically polished section. Interference layering and light polarization techniques were used to obtain contrast.
[c] Determined from optical ellipsometry.
[d] Determined from x-ray diffraction pattern.
[e] Determined from four-contact method, Ag paste contacts, exhange gas chamber.

I-d. X-RAY DIFFRACTION

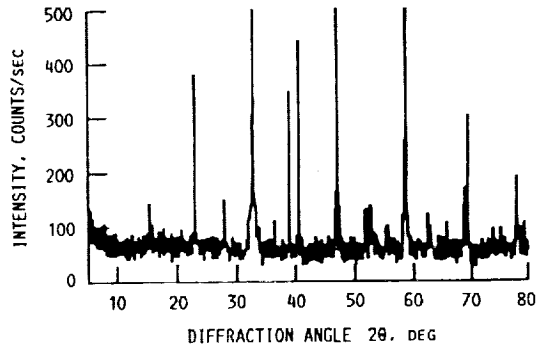

I-c. OPTICAL ELLIPSOMETRY

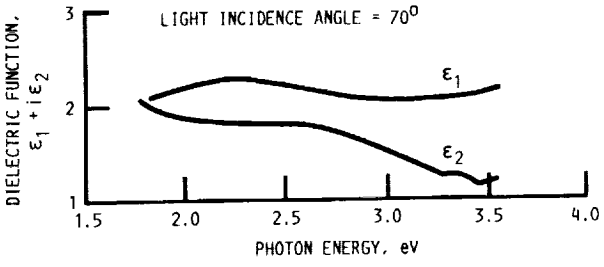

I-e. RESISTANCE VS TEMPERATURE

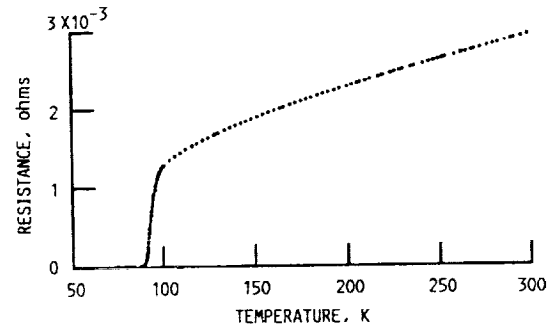

Radiography

Conventional x-ray radiography was used to examine the YBCO specimen for gross porosity variation. Film radiographic techniques are capable of resolving porosity variations on the order of 3 percent in ceramics (ref. 58). Briefly, x-rays are attenuated exponentially by matter, and their transmitted intensity can be expressed as

$$I = I_o \exp\left[\left(\frac{-\mu}{\rho}\right)(\rho x)\right] \tag{2}$$

where I_o is the original beam intensity, μ/ρ is the mass attenuation coefficient (cm^2/g), μ is the linear attenuation coefficient (cm^{-1}), ρ is the density (g/cm^3), and x is the section thickness (cm) (ref. 59). When x-raying a specimen, second-phase regions (including pores) having mass attenuation coefficients different from the matrix generally show up as different gray levels on video or film if present in large enough concentrations along the path of the x-ray beam.

Radiographs were made through the thickness of the YBCO disk with conventional contact methods, under optimized conditions, to obtain the most accurate, highest contrast prints. The radiographs were made with a tungsten source (target) and beryllium window. The source-to-disk distance was approximately 3 ft, and the exposure conditions were 120 kV, 5 mA, and 11 to 12 min. The disk was masked with lead and covered with thin lead screens to offset the effects of x-ray scattering from the sample edges and lead mask, respectively.

Figure 2 shows a radiograph film of the YBCO disk. The outlined region in the radiograph indicates the region of the YBCO disk that was scanned with the ultrasonic scanning system. This area was relatively free of microcracks. Careful examination of both the radiograph negative and film revealed no definite grey scale variation. Therefore, if any porosity variations are present, they are apparently below the detectability limit of conventional radiography for this material.

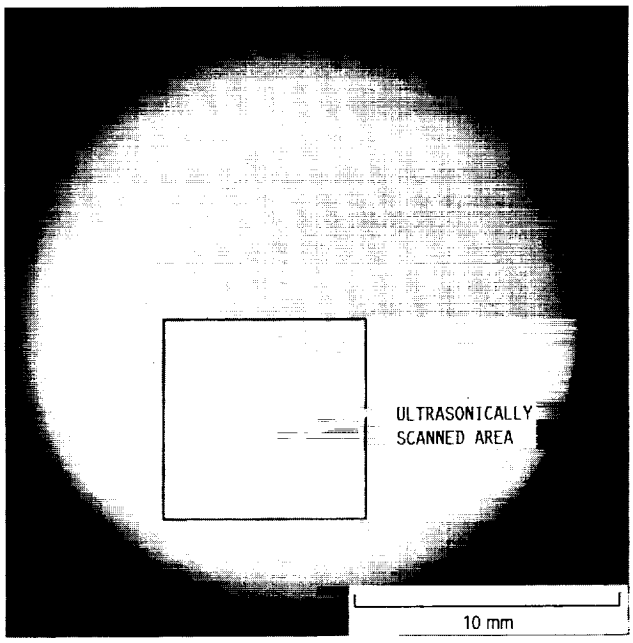

Figure 2.—X-ray radiograph film of YBCO disk. Highlighted square region outlines ultrasonically scanned area.

Ultrasonic Imaging

Velocity measurement.—The pulse-echo contact technique (refs. 16 and 60) illustrated in figure 3, parts (a) and (b), was used to obtain ultrasonic waveform data. The technique is described as follows. A single broadband ultrasonic pulse (main pulse) is excited (via the crystal) in the buffer rod. The pulses labeled FS_1' and FS_2 in figure 3(a) are the first front surface reflections without and with the specimen present on the buffer rod, respectively. With the sample in place on the buffer rod, the ultrasonic pulse is partially reflected at the buffer rod-couplant-sample (BCS) interface. The main ultrasonic pulse travels forward through the sample and then reflects off the back surface of the sample and again interacts with the BCS interface. In this journey (twice the specimen thickness), the ultrasonic pulse more or less integrates the microstructural information in the volume element sampled. Echo B_1' is partially reflected at the BCS interface and is subsequently reflected again at the back surface. The second back-surface reflection is labeled B_2'. Echoes B_1' and B_2' are not directly measurable in this experimental configuration. Their reduced waveform amplitudes, labeled B_1 and B_2 in figure 3(b), are measurable.

Reproductions of actual waveforms FS_2, B_1, and B_2 that were obtained from a point near the center of the ultrasonically scanned region (see fig. 2) are shown in figure 3(c). Each is the average of 64 acquisitions. The back-surface-reflected ultrasonic pulses B_1 and B_2, altered by the microstructural information in the volume element probed, were used to calculate cross-correlation velocity (refs. 60 and 61) at that scan point. Cross correlation is essentially a mathematical formulation of echo overlap (refs. 60 and 62) where similar features of two waveforms that were produced from the same initial excitation, but shifted in time, are matched. In this manner, the time shift (delay) between the two waveforms can be precisely determined. Cross-correlation velocity is given by

$$V = \frac{2x}{\tau_o} \tag{3}$$

where τ_o is the time shift for which

$$\left| lim_{T\to\infty} \int_{-T}^{T} B_1(t) \bullet B_2(t+\tau)\, dt \right| \quad -\infty \le \tau \le \infty \tag{4}$$

reaches a maximum value. Here x is the sample thickness, V is the velocity, t is time, T is the time extent (width) of the pulse, and τ is the time shift.

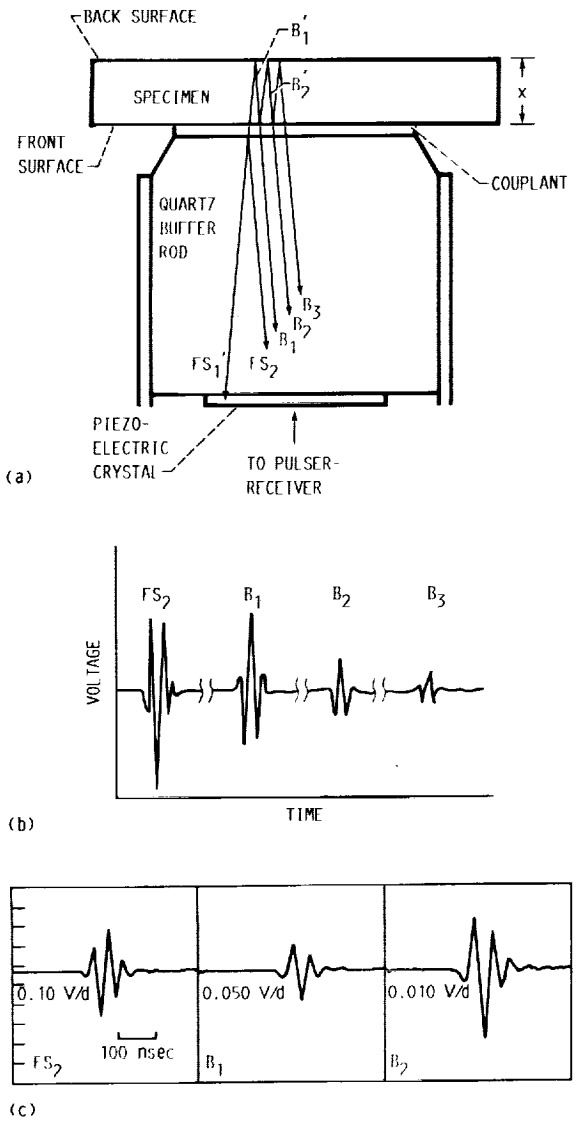

(a) Diagram of transducer/specimen configuration for pulse-echo ultrasonics.
(b) Resulting waveforms.
(c) Reproductions of actual ultrasonic waveforms obtained near center of ultrasonically scanned region of YBCO disk; V/d = volts/division.

Figure 3.—Pulse-echo contact technique and reproductions of actual resulting waveforms.

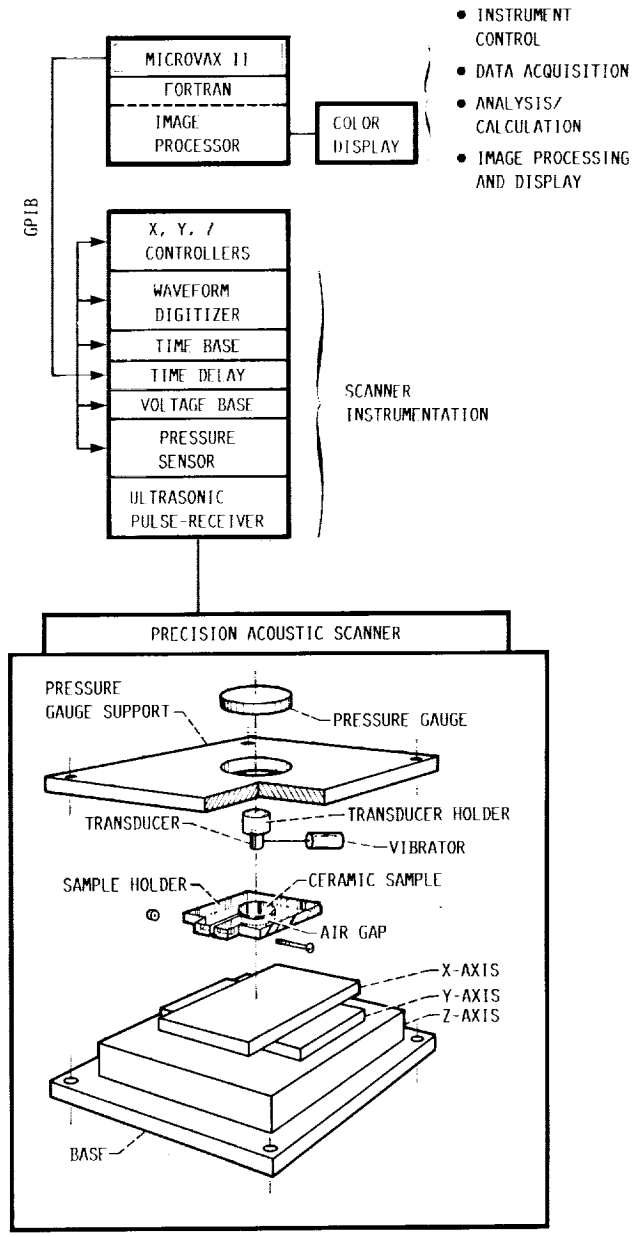

Figure 4.—Computer-controlled precision acoustic scanning system (PASS).

Cross correlation is a preferred method of determining velocity since it produces accurate velocities even with noisy signals. (Nevertheless, minimally distorted ultrasonic pulses of high signal-to-noise ratio are desirable.)

Scan system. —A schematic of the PASS is shown in figure 4. The YBCO disk was mounted in a Lucite (Dupont) holder, as shown in figure 4, with the polished side of the disk facing upward. The holder was mounted on x-, y-, and z-microscanning positioner tables, each having a step resolution of 1.0 μm. A 20-MHz broadband longitudinal wave transducer driven by a pulser-receiver having a bandwidth of 1 to 150 MHz generated the ultrasonic pulse. The transducer had an 11/16-in.-diam buffer rod and a 1/4-in.-diam piezoelectric crystal. A displacement pressure gauge was mounted over the transducer to control the contact pressure of the transducer on the disk. The contact pressure was 5 ± 1 lb. A nonaqueous couplant was used between the disk and buffer rod.

A Digital Equipment Corp. Microvax II minicomputer (see fig. 4) was used to control movement of the microscanning tables, acquire the raw ultrasonic waveforms, and calculate velocity (ref. 18). Image processing hardware and software that was interfaced with the computer allowed construction and display of the velocity measurements of the scanned area in the form of an image.

Image. —Raw waveform data were acquired by using the PASS at room temperature at 100-μm increments over the 8-

by 8-mm area of the YBCO disk outlined in the radiograph of figure 2. (Actually, a volume defined by this area was ultrasonically interrogated.) An 81- by 81-point data grid was obtained. Figure 5(a) shows the image constructed from ultrasonic velocity values obtained at each scan point. A continuous scale consisting of 256 shades of color allowed the display of subtle velocity changes across the disk. The highest, lowest, and mean velocities measured across the scanned region of the disk were 0.516, 0.510, and 0.512 cm/μsec, respectively. No recognizable pattern of velocity variation is apparent (e.g., lowest velocities and highest velocities located in the central and outer portions of the region, respectively, as has been seen for SiC specimens (ref. 32)). The highest velocities occur in the central far right and upper far right, whereas the lowest velocities occur in the lower right corner of the scanned region. The large area extending from the upper central to the lower central portion of the scanned region shows velocities near the mean. The image shows a small total velocity variation, on the order of 1 percent, across the scanned region. The 1-percent total variation is smaller than the 2.6-percent variation previously seen for high-density SiC structural ceramic specimens (ref. 16).

Figure 5(b) shows optical photomicrographs of cross-sectional thicknesses obtained from the ultrasonically interrogated volume of the YBCO disk. Porosity, indicated by the black spots in the photomicrographs, varies throughout the disk (within each cross section and from cross section to cross section). However, accurate and precise quantitative differences in pore concentration are difficult to determine practically from the optical information. In addition, only two-dimensional porosity information is available from the photomicrographs. The dashed arrows in figure 5 point from the thickness cross sections to the corresponding horizontal location within the velocity image.

Discussion

The ultrasonic velocity image in figure 5(a) can be thought of as a two-dimensional projection representing relative pore concentration values for the volume of sample scanned. As shown in figure 1, a 1-percent velocity variation very likely corresponds approximately to a 1-percent porosity variation in the YBCO specimen. The image is believed, for several reasons, to provide a precise and accurate measure of relative pore concentration (insofar as reproducibility and approaching true value, respectively, are concerned). Considering accuracy, the experimental sample was shown to be single-phase, randomly textured, and free of nonuniform residual microstress, thereby leaving porosity as the varying microstructural element. Because there is an absence of interpenetrating porosity channels and significant microcracks, it is unlikely that an appreciable layer of impurity phase(s) was formed at the surface of the YBCO disk or that liquid couplant diffused into the disk during the investigation. These events, if they had occurred, could have affected the accuracy of ultrasonic measurements (refs. 5 and 63). Furthermore, although the 100-μm index size used in the scan procedure

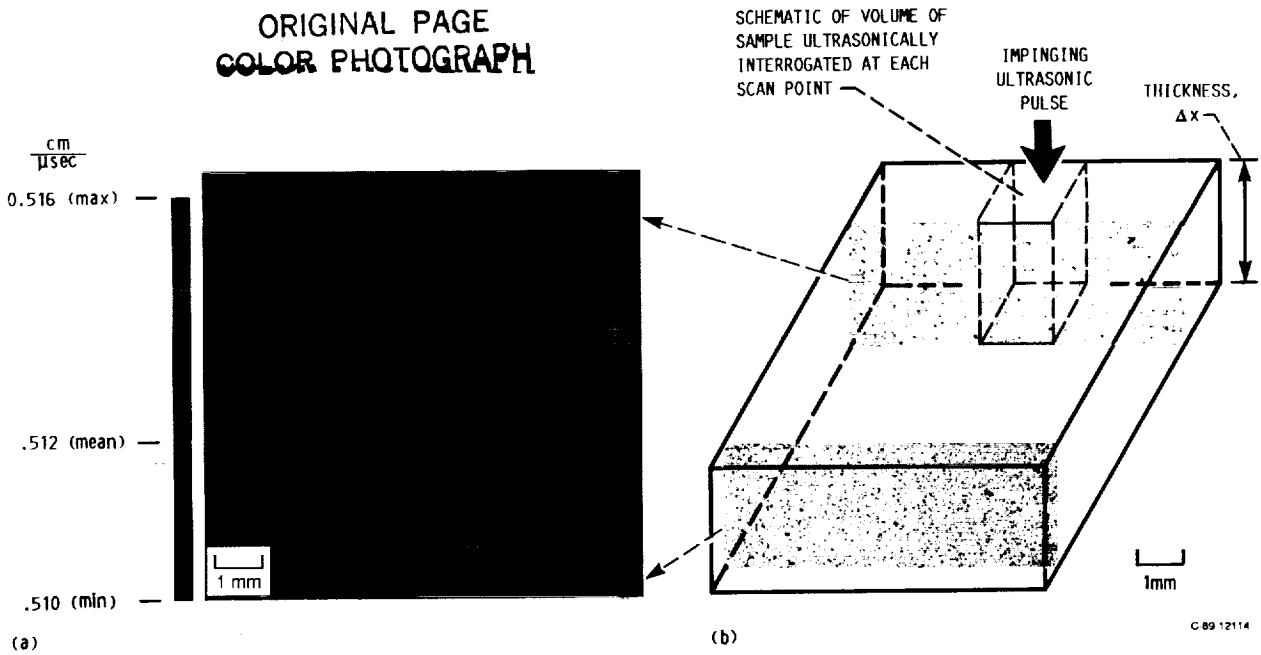

(a) Velocity image constructed from ultrasonic scan data obtained over 8- by 8-mm region of the YBCO disk.
(b) Optical photomicrographs of thickness cross sections from ultrasonically scanned volume, showing porosity variations. Black spots indicate porosity. Dashed arrows point from thickness cross sections to corresponding horizontal location within velocity image.

Figure 5.—Ultrasonic velocity image showing subtle porosity variations present in the scanned region of the YBCO disk.

is approximately an order of magnitude smaller than the transducer beam diameter, scanning on a finer scale than the beam diameter resulted in approximately four times greater resolution of structural detail (pore concentration variations). The scan increment used in this investigation was 10 times smaller than that used in reference 16. Finally, the raw waveforms B_1 and B_2 shown in figure 3(c), each the average of 64 acquisitions, are undistorted and free of noise, thereby leading to high confidence in the cross-correlation velocity determination. Concerning precision, in a second scan of the same region, the identical ultrasonic image was obtained within the uncertainty of the velocity measurement. This uncertainty was conservatively calculated at 0.36 percent, taking into account the errors inherent in the sample thickness and the time delay measurements.

The authors recognize that for most potential commercial applications YBCO will be a thin film, textured bulk, or single crystal, since J_c is usually an order of magnitude higher in these forms than it is in the untextured bulk material. However, improvements in processing methods may result in high-J_c untextured material of commercial interest. In addition, for uniformly textured YBCO, texture variation is removed as a variable affecting velocity. In this instance, the global porosity distribution can be imaged if the material is single-phase and free of nonuniform residual stress.

The PASS technique should also be useful for tracking time-dependent environmental degradation in YBCO caused by chemical attack or thermal stresses. Thermal cycling from room temperature to application temperature (77 K) may cause additional porosity in the form of microcracks. A velocity decrease in the cracked regions may be detectable and quantified. YBCO is known to react with water and other compounds (refs. 51 and 52) to form nonsuperconducting phases (such as $BaCO_3$, CuO, and $Ba(OH)_2$). If YBCO is exposed to reactive conditions, the velocity in the degraded material that contains reaction products may be different than in the original superconducting material. Finally, precision acoustic scanning can be useful for comparing the homogeneity of superconducting ceramics processed by different methods.

Conclusion

This study reports on characterization of global porosity variation within a nominally 93-percent-dense specimen of $YBa_2Cu_3O_{7-x}$ high-temperature superconductor. With a computer-controlled scanning system, ultrasonic velocity measurements were obtained at 100-μm increments over an 8- by 8-mm area of the $YBa_2Cu_3O_{7-x}$ specimen. The measurements were used to form a color image of velocity variation across the scanned region of the specimen. Subtle velocity variation on the order of 1 percent was observed. The specimen was shown by experimental methods to be single-phase, untextured, and free of nonuniform residual microstress. From this knowledge and an established velocity-density relationship, a conclusion may be drawn that the observed velocity variations are very likely due solely to porosity variations of similar magnitude. Locating these subtle porosity variations is critical since they can result in an order of magnitude variation in J_c for dense YBCO specimens. Thus, mapping the global porosity distribution within YBCO may reveal regions that have poorer superconducting properties.

Acknowledgments

The authors wish to thank T.A. Leonhardt of Sverdrup Technology, Inc., NASA Lewis Research Center Group, for careful sample preparation and metallography; Professor M.R. DeGuire of Case Western Reserve University for thought-provoking discussion, critical reading of the manuscript, and other general assistance; and Dr. S.A. Alterovitz of NASA Lewis Research Center for assistance concerning optical ellipsometry.

Lewis Research Center
National Aeronautics and Space Administration
Cleveland, Ohio 44135
November 14, 1988

References

1. J.G. Bednorz and K.A. Muller, Zeit Phys. B, **64**, 189 (1986).
2. P.H. Chu, P.H. Hor, R.L. Meng, L. Gao, Z.J. Huang, J.R. Wu, Y.Q. Wang, and C.J. Huang, Phys. Rev. Lett., **58**, 911 (1987).
3. H. Maeda, Y. Tanaka, M. Fukutomi, and T. Asano, Jpn. J. Appl. Phys. Lett, **27**, L209 (1988).
4. N.MCN. Alford, W.J Clegg, M.A. Harmer, and J.D. Birchall, Nature, 332, **58** (1988).
5. N.MCN, Alford, J.D. Birchall, W.J. Clegg, M.A. Harmer, and K. Kendall, Ceramic Superconductors II, edited by Man F. Yan (American Ceramic Society 1988), p. 232.
6. J.E. Blendell, C.K. Chiang, D.C. Crammer, S.W. Freiman, E.R. Fuller, Jr., E. Drescher-Krasicka, and M.L. Johnson, Adv. Ceram. Mater., **2**, 512 (1987).
7. M.J. Cima and W.E. Rhine, Adv. Ceram. Mater., **2**, 329 (1987).
8. J.W. Ekin, Adv. Ceram. Mater., **2**, 586 (1987).
9. H.M. Ledbetter, M.W. Austin, S.A. Kim, and M. Lei, J. Mater. Res., **2**, 786 (1987).
10. D. Shi, D.W. Capone II, G.T. Goudey, J.P. Singh, N.J. Zaluzec, and K.C. Goretta, Sintering of $YBa_2Cu_3O_{7-x}$ Compacts, to be published.
11. S.N. Song, S.-J. Hwu, F. Du, K.R. Poeppelmeier, T.O. Mason, and J.B. Ketterson, Adv. Ceram. Mater., **2**, 480 (1987).
12. W.D. Kingery, H.K. Bowen, and D.R. Uhlman, Introduction To Ceramics (John Wiley / Sons, Inc., 1976), p. 9.
13. H.M. Ledbetter, N.V. Frederic, and M.W. Austin, J. Appl. Phys., **51**, 305 (1980).
14. J.W. McCauley, in Nondestructive Testing of High-Performance Ceramics; edited by A. Vary and J. Snyder (American Ceramic Society, 1987), p. 1.
15. A.F. Hepp and J.R. Geller, Mater. Res. Bull., **23**, 693 (1988).
16. E.R. Generazio, Mater. Eval., **46**, 1198 (1988).
17. E.R. Generazio, D.B. Stang, and D.J. Roth, J. Am. Ceram. Soc., **72**, 1282 (1989) (NASA TM-101340).

18. E.R. Generazio, D.B. Stang, and D. Roth, NASA TM-4106 (1989).
19. A.L. Gaiduk, S.V Zherlitsyn, O.R. Prikhod'ko, and V. Fil', Sov. J. Low Temp. Phys., **14**, 395 (1988).
20. M.R. DeGuire and D.E. Farrell, Adv. Ceram. Mater., **2**, 593 (1987).
21. D.C. Larbalestier, M. Daeumlin, X. Cai, X.J. Seuntjens, J. McKinnel, D.P. Hampshire, P. Lee, C. Meingast, T. Willis, and H. Muller, J. Appl. Phys., **62**, 3308 (1987).
22. D. Saint-James, G. Sarma, and E.J. Thomas, Type II Superconductivity (Pergamon Press, 1969), p. 214.
23. D.P. Hampshire, X. Cai, X.J. Seuntjens, and D.C. Larbalestier, Supercond. Sci. Technol., **1**, 12 (1988).
24. A.P. Malozemoff, Y. Yeshurin, and T.K. Wortington, Cryogenics (Suppl), **29**, 258 (1989).
25. D.R. Nelson, Phys. Rev. Lett., **60**, 1973 (1988).
26. J. Evetts, "The Relation of Critical Current Irreversibility to Trapped Flux and Microstructure in Polycrystalline $YBa_2Cu_3O_{7-x}$," to be published in Cryogenics, (1989).
27. H. Kupfer, Investigation of Inter- and Intragrain Critical Currents in High-T_c Ceramic Superconductors," to be published in Cryogenics, (1989).
28. R. Rose, in The Science and Technology of Superconductivity, edited by W.D. Gregory and W.N. Mathews (Plenum Press, 1973), p. 289.
29. J. Ekin, in Superconductor Materials Science, (Plenum Press, 1981), p. 455.
30. G.Y. Baaklini and P.B. Abel, Mater. Eval., **46**, 1477 (1988).
31. E.G. Evans, B.R. Tittman, and L. Ahlberg, J. Appl. Phys., **49**, 2669 (1978).
32. E.R. Generazio, Mater. Eval., **46**, 1198 (1988).
33. R.S. Gilmore, K.C. Tom, J.D. Young, and D.R. Howard, Phil. Trans. R. Soc. Lond. A, **320**, 215 (1986).
34. J.J. Gruber, J.M. Smith, and R.H. Brockelman, Mater. Eval. **46**, 90 (1988).
35. S.J. Klima, G.K. Watson, T.P. Herbell, and T.J. Moore, NASA TM-82765 (1981).
36. D.J. Roth, E.R. Generazio, and G.Y. Baaklini, Mater. Eval., **45**, 958 (1987).
37. D.C. Kunerth, K.L. Telschow, and J.B. Walter, Mater. Eval., **47**, 571 (1989).
38. S. Wang and L. Adler, Review of Progress in Quantitative Nondestructive Evaluation, Vol. 3B, edited by D.O. Thomson and D.E. Chimenti (Plenum Press, 1989), p. 1211.
39. J. Dominec, Sound Attenuation and Velocity in Superconductive Ceramics, to be published in Superconductor Science and Technology (1989).
40. R.W. Rice, Treatise on Materials Science & Technology, Volume 11, edited by R.K. MacCrone (Academic Press, 1977), p. 199.
41. G.V. Blessing, N.N. Hsu, and T.M. Proctor, Nondestructive Methods for Material Property Determination, edited by C.O. Ruud and R.E. Green, Jr. (Plenum Press, 1984), p. 353.
42. J.R. Frederick, Ultrasonic Engineering (John Wiley and Sons, Inc., 1965), p. 237.
43. D. Husson, S.D. Benett, and G.S. Kino, Nondestructive Methods for Material Property Determination, edited by C.O. Ruud and R.E. Green, Jr. (Plenum Press, 1984), p. 365.
44. S. Ewert, S. Guo, P. Lemmens, F. Stellmach, and J. Wynants, Solid State Communications, **64**, 1153 (1987).
45. V. Ramachandran, G.A. Ramadass, and R. Srinivasan, Physica C, 153-155, 278 (1988).
46. M. Suzuki, Y. Okuda, I. Iwasa, A.J. Ikushima, T. Takabatake, and M. Ishikawa, Physica C, 153-155, 266 (1988).
47. K.J. Sun, M. Levy, B.K. Sarma, P.H. Hor, R.L. Meng, Y.Q. Wang, and C.W. Chu, Physics Lett. A, **131**, 541 (1988).
48. R. Round and B. Bridge, J. Mater. Sci. Lett., **6**, 1471 (1987).
49. F. Hellman, E.M. Gyorgy, D.W. Johnson, Jr., H.M. O'Bryan, and R.C. Sherwood, J. Appl. Phys., **63**, 447 (1988).
50. C., Kittel, Introduction to Solid State Physics, (John Wiley / Sons, Inc., 1986), p. 321.
51. K.G. Frase, E.G. Liniger, and D.R. Clarke, Adv. Ceram. Mater. **2**, 698 (1987).
52. M.E. Yan, R.L. Barns, H.M. O'Bryan, Jr., P.K. Gallagher, R.C. Sherwood, and S. Jin, Appl. Phys. Lett., **51**, 532 (1987).
53. V. Alreja and J.M. Liu, Nondestructive Methods for Material Property Determination, edited by C.O. Ruud and R.E. Green, Jr. (Plenum Press, 1984), p. 39.
54. B.D. Cullity, Elements of X-ray Diffraction (Addison-Wesley Publishing Company, Inc., 1984), p. 286, 447.
55. W. Wong-Ng, H.F. McMurdie, B. Paretzkin, Y Zhang, K.L. Davis, C.R. Hubbard, A.L. Dragoo, and J.M. Stuart, Powder Diffraction, **2**, 191 (1987).
56. M.K. Kelly, S-W, Chan, K. Jenkin II, D.E. Aspens, P. Barboux, and J.-M. Tarason, Appl. Phys. Lett., **53**, 2333 (1988).
57. B.I. Khuri-Yakub, Y. Shui, G.S. Kino, D.B. Marshall, and A.G. Evans, Review of Progress in Quantitative Nondestructive Evaluation, Vol. 3A, edited by D.O. Thompson and D.E. Chimenti (Plenum Press, 1984), p. 229.
58. S.J. Klima and G.Y. Baaklini, NASA CP-2383 (1984), p. 117.
59. G.Y. Baaklini and D.J. Roth, J. Mater. Res., **1**, 457 (1986).
60. D.R. Hull, H.E. Kautz, and A. Vary, Mater. Eval., **43**, 1455 (1985).
61. R.N. Bracewell, The Fourier Transform and Its Applications (McGraw-Hill, 1986).
62. E.P. Papadakis, J. Acoust. Soc. Am., **42**, 1045 (1967).
63. D.P. Almond, E. Lambson, G.A. Saunders, and W. Hong, J. Phys. F.: Met. Phys., **17**, L221, 261 (1987).

NASA
National Aeronautics and Space Administration

Report Documentation Page

1. Report No.	2. Government Accession No.	3. Recipient's Catalog No.
NASA TM-102130		

4. Title and Subtitle

Subtle Porosity Variation in the $YBa_2Cu_3O_{7-x}$ High-Temperature Superconductor Revealed by Ultrasonic Imaging

5. Report Date

January 1990

6. Performing Organization Code

7. Author(s)

D.J. Roth, E.R. Generazio, D.B. Stang, and A.F. Hepp

8. Performing Organization Report No.

E-4917

10. Work Unit No.

506-43-11

9. Performing Organization Name and Address

National Aeronautics and Space Administration
Lewis Research Center
Cleveland, Ohio 44135-3191

11. Contract or Grant No.

13. Type of Report and Period Covered

Technical Memorandum

12. Sponsoring Agency Name and Address

National Aeronautics and Space Administration
Washington, D.C. 20546-0001

14. Sponsoring Agency Code

15. Supplementary Notes

D.J. Roth, E.R. Generazio, A.F. Hepp, NASA Lewis Research Center; D.B. Stang, Sverdrup Technology, Inc., NASA Lewis Research Center Group, Cleveland, Ohio 44135.

16. Abstract

This study reports on characterization of global porosity variation within a nominally 93-percent-dense specimen of $YBa_2Cu_3O_{7-x}$ high-temperature superconductor. With a computer-controlled scanning system, precision ultrasonic velocity measurements were obtained at 100-μm increments over an 8- by 8-mm area of the $YBa_2Cu_3O_{7-x}$ specimen. The measurements were used to form a color map of velocity variation across the scanned region of the specimen. Subtle velocity variation on the order of 1 percent was observed. The specimen was shown by experimental methods to be single-phase, untextured, and free of nonuniform residual microstresses. From this knowledge and an established velocity-density relationship, a likely conclusion is that the observed velocity variations are solely due to porosity variations of similar magnitude. Locating these subtle porosity variations is critical since they can result in an order of magnitude variation in J_c for dense YBCO specimens. Thus, mapping the global porosity distribution within $YBa_2Cu_3O_{7-x}$ may reveal regions that have poorer superconducting properties. In this study ultrasonic velocity results are translated into useful microstructural information for the material scientist.

17. Key Words (Suggested by Author(s))	18. Distribution Statement
Ultrasonic velocity; High-T_c superconductor; Ytrium-barium-copper oxide; Porosity; Ultrasonics; Microstructural variability; Nondestructive evaluation	Unclassified – Unlimited Subject Category 38

19. Security Classif. (of this report)	20. Security Classif. (of this page)	21. No of pages	22. Price*
Unclassified	Unclassified	10	A02

*For sale by the National Technical Information Service, Springfield, Virginia 22161